Available online at www.sciencedirect.com
SCIENCE DIRECT®
Journal of Non-Crystalline Solids 351 (2005) 1532–1542
JOURNAL OF NON-CRYSTALLINE SOLIDS
www.elsevier.com/locate/jnoncrysol

Molecular dynamics studies of brittle fracture in vitreous silica: Review and recent progress

Krishna Muralidharan [a,*], J.H. Simmons [a], P.A. Deymier [a], K. Runge [b]

[a] Department of Materials Science and Engineering, University of Arizona, Tucson, AZ 85721, USA
[b] Quantum Theory Project, University of Florida, Gainesville, FL 32611, USA

Abstract

The dynamics of brittle fracture in vitreous silica has been a subject of many molecular dynamics (MD) simulations and experiments. A striking similarity between both simulations and experiments is the observation of nanoscale voids that eventually coalesce leading to failure. In this work, we review the above MD simulations and carry out further MD investigations using two variations of classical 2-body potentials. We study the effect of charge-transfer, an important aspect neglected by previous simulations. Further, we examine the growth of 'critical' voids and characterize regions surrounding the voids.

1. Introduction

Fracture in brittle materials results from the sudden and rapid propagation of sub-micron level defects/cracks under the influence of a local stress field. These local stress fields are significantly higher than the macroscopic stress applied, causing local rearrangement of atoms around the crack tip and a consequent straining of atomic bonds that ultimately break, leading to separation of the material. Early modeling efforts to study the brittle fracture process, pioneered by Griffith [1], and improved by Irwin [2] and Barenblatt [3], were based on analytical continuum mechanics. These methods could accurately predict the initiation of fracture as well as calculate the energetics of the process, but lacked the versatility to account for atomic dynamics in high-stress regions. With the advent of powerful computers, high-speed, high-resolution atomistic computation techniques like molecular dynamics (MD) became the preferred modeling tool of investigators. MD investigations of the fracture process in brittle materials have been carried out extensively [4–14], and the proposed models that describe brittle fracture have been fairly consistent with experimental findings [15,16]. In this paper, we plan to review past MD simulations that have looked at the fracture process of a prototypical brittle material – vitreous or amorphous (a) silica (a-SiO_2), and then address some of the issues that have been previously ignored.

2. Vitreous silica – a prototypical brittle material

The structure of a-SiO_2 is an open network of silica tetrahedra, with each tetrahedron linked to its neighboring tetrahedra via a bridging oxygen (corner-sharing). Experimental brittle fracture studies of silica glass have yielded a number of properties that are characteristics of an 'ideal' brittle material. Specifically, a-SiO_2 exhibits the 3-regime behavior as described by Wiederhorn

* Corresponding author.
E-mail address: krishna@qtp.ufl.edu (K. Muralidharan).

0022-3093/$ - see front matter © 2005 Elsevier B.V. All rights reserved.
doi:10.1016/j.jnoncrysol.2005.03.026

[17,18]. Fracture processes of regimes-1 and -2 are limited by environmental effects (slow crack growth), whereas in type-3 fracture, the material becomes unstable under the applied stress without regard to environmental effects and the high crack growth velocities that result are limited only by the mechanical properties of the material (sudden fracture). Procter et al. [19] measured the strength of ultra-pure silica fibers (without surface flaws) to be 18.0 GPa, about two orders of magnitude higher than the measured strength of bulk silica. Maximum crack velocities during regime-3 fracture, have also been calculated and have been reported to be anywhere between 40% and 60% of the speed of sound [20].

3. Molecular dynamics (MD)

Molecular dynamics methods are very orthodox means for simulating molecular-scale models of matter [21]. The essence of MD methods involves solving the N-body problem of classical mechanics. In other words, it involves solving periodically the Newton's equations of motions for a given set of interacting particles (the interactions between particles governed by an interatomic potential), enabling one to keep track of the evolution of the system in phase space. The equations of motions are solved using standard finite difference schemes at each time step of the simulation. An MD simulation can be carried out under a variety of constant thermodynamic conditions like total energy E, pressure P, volume V, temperature T, number of atoms N or chemical potential μ. Typical MD simulations employ periodic boundary conditions (PBC) to avoid surface effects. The principal advantages of MD simulations are that one could very precisely obtain static and dynamic properties of the simulated systems provided the interatomic potential describes the atomic interactions accurately. Classical MD simulations do not explicitly treat electronic effects, and therefore cannot adequately handle regime-1 and -2 fracture, where physisorption and chemisorption processes control fracture. However, MD is particularly suited to study environment independent fast fracture (regime-3) as it can keep track of the extensive atomic rearrangements that occur around the crack tip, without having to account for chemical reactions at the crack tip as the crack propagates. Researchers have used quantum mechanical calculations to study environment induced fracture [22–24] as well as to obtain the energetics of the fracture process [25] and have also tried to combine higher-level electronic calculations in conjunction with MD to have a better description of the system. These 'combination' methods have their deficiencies and will not be discussed in this paper.

4. Interatomic potentials for silica

As pointed out earlier, the exactness of MD simulations is dictated by the accuracy of the interatomic potentials being used. A plethora of interatomic potentials are available to model the different structures of silica. Most of them are empirical and are fitted to a wide variety of parameters in order to represent silica. Erikson and Hosteler [26] as well as Schaible [27] have described the existing silica potentials in their respective articles. Thus, in this paper, we will only review a handful of potentials used by researchers who have looked at the mechanical properties of a-SiO_2.

An essential requirement for a reliable silica potential is to ensure the stability of the silica tetrahedron and capture the partial ionic–partial covalent nature of the Si–O bond. In addition, it should satisfactorily model the various polymorphs of silica. Some of the successful potentials comprise of only 2-body terms, and others use a combination of 2-body and 3-body terms. Many of these potentials are derived from the functional form of the Born–Mayer–Huggins (BMH):

$$\phi_{ij} = \frac{q_i q_j}{r_{ij}} + A_{ij} e^{-b_{ij} r_{ij}} + C_{ij} r_{ij}^{-6} + D_{ij} r_{ij}^{-8}.$$

In the above equation, ϕ_{ij} represents the interaction potential between atom i and j, r_{ij} equals the separation distance between i and j, q_i and q_j are the charges on atoms i and j. A_{ij}, b_{ij}, C_{ij} and D_{ij} correspond to potential parameters. The latter two terms in the above equation represent multipole terms and can be neglected if the atoms are not highly polarizable-modified BMH potential (mBMH).

Woodcock et al. [28] were among the first to do simulations of silica. They used the mBMH potential which was fitted to the experimental radial correlation function of the glass. Soules used a similar approach to derive the S-potential, and used a cutoff of 5.5 Å. The S-potential was successful in its ability to simulate vitreous silica structures with approximately the correct density. The simulated pair correlation functions had good agreement with experimental neutron diffraction data [29]. Mitra et al. [30–32] also used 2-body representations in their potential formulation, the potential parameters being fitted to the short-range structure and melting temperatures of β-cristobalite. The above described potentials (exclusively 2-bodied) were unable to describe the experimental Si–O–Si angle distribution exactly and yielded distributions much broader than experiment [33]. Thus researchers added 3-body terms to existing potentials and were able to force the distribution to be more realistic. The Vessal potential [35], the Vashishta (V) potential [34] and the Feuston–Garofalini (FG) potential [33] are some of the successful, widely used 3-body potentials.

The functional form of the FG potential uses a combination of the mBMH potential and the 3-body term of the Stilinger–Weber potential [30]. The FG potential has a weaker repulsion in the Si–Si and O–O interactions when compared with the S-potential. It has the functional form

$$\phi_{ij2} = A_{ij}e^{(-r_{ij}/\rho)} + \frac{q_i q_j}{r_{ij}}\operatorname{erfc}\left(\frac{r_{ij}}{\beta}\right),$$

$$\phi_{ijk3} = \lambda \exp\left(\frac{\gamma}{r_{ij}-r^c} + \frac{\gamma}{r_{jk}-r^c}\right)[\cos\theta_{ijk} - \cos\theta^c]^2,$$

where the parameters are the same as in Ref. [33]. The V-potential included the electronic polarizability of the constituent ions in its representation. The Vessal potential includes 40 adjustable parameters and claims an excellent fit to experimentally measured properties of various phases of silica. Wright [36] deduced that the V-potential and the Vessal potential have the best fit to neutron diffraction data of any simulated structures at the time of comparison.

Almost all of the above potentials were empirically derived, the parameters chosen to fit experimental data. The effective charges on Si and O were also chosen empirically and were based on experimental observations. Tsuneyuki et al. (TTAM) [37] and van Beest et al. (BKS) [38] were the first to use ab initio cluster calculations and independently determined the optimal normalized charges on Si and O to be +2.4 and −1.2. Both TTAM and BKS potentials have been successful in modeling many silica polymorphic phases [39–43]. BKS differs from TTAM in the fact that it ignores the Si–Si short-range interactions. Even though both TTAM and BKS are able to represent the equilibrium structures of silica, they do not accurately reproduce the vibrational properties of silica [41,44].

4.1. Charge-transfer potentials

The above discussed potentials assume that the effective charges associated with silicon and oxygen are fixed and do not vary as a function of their immediate environment. This assumption is not necessarily true when systems are far away from equilibrium, and could lead to erroneous results while modeling fracture, as the process is accompanied by extensive bond breakage and a consequent rearrangement of atoms. Alavi et al. [45] proposed a scheme to treat the charge-transfer processes in an explicit way. The scheme used ensures that the charge-transfer forces are conservative and no numerical instabilities have been observed when used in conjunction with the BKS potential. Streitz and Mintmire [46] developed a computational method for MD simulations, which explicitly included variable charge-transfer between anions and cations. This method was developed to study metal oxides and could describe the elastic properties, surface energies and surface relaxation of the metal oxides very accurately. In this method, the effective charge on each atom is chosen such that the total electrostatic energy is minimized at each time step of the simulation. Valone and Atlas [47] in a very recent paper have devised a new charge-dependent pair potential that uses chemical potential equalization to dynamically adjust the charges of constituents, similar in spirit to the method of Streitz and Mintmire, but more self-consistent as pointed out in the paper. Huang and Keiffer [44] developed a potential that accounted for explicit charge-transfer upon breaking and forming chemical bonds. They were able to describe the thermally induced α- to β-cristobalite transformation very well.

5. MD and brittle fracture in a-SiO_2

The mechanical properties of silica have been subject to many MD investigations. Some of the work involved studying the effects of pressure on silica (documented in Ref. [21]) and will not be discussed in this paper. We will review the studies that have looked at a-SiO_2 under tensile stress and (or) negative pressure. An important point to be noted is that in all of the studies under review, the influence of the environment has been ignored and the silica system is assumed to be in vacuum.

Soules and Busby [4] used MD with the S-potential to look at sodium silicate glass under both tension and compression. They studied systems of approximately 1000–2000 atoms with free surfaces, and subjected them to both uniaxial and biaxial expansions. Under biaxial expansion, the sample was drawn thinner, and when the expansion was large, the sample failed via cavitation. When the sample was under uniaxial strain, the strain applied by displacing the atoms close to the surface, atomic bonds were initially elastically stretched, followed by considerable plastic deformation. A flaw was then formed, finally resulting in separation. The stress–strain curves showed that fracture was brittle as the resisting material tensile stress decreased rapidly past the maximum stress point. These authors compared the behavior of the sample at room temperature as well as 625 K and obtained similar results. An introduction of atomic-level defects did not play any role in the sample response to both uniaxial and biaxial expansions.

Keiffer and Angell [48] catastrophically ruptured the a-SiO_2 structure by the application of negative pressure (isotropic expansion) in their MD simulations. This caused bond-angle opening without rupture up to a maximum tensile limit. Beyond this limit, the structure ruptured in a very specific way, by developing a self-similar void structure. This structure was described well by a fractal dimension which changed linearly with density. They chose the BMH functional form to represent atomic interactions.

Ochoa and Simmons [6] were the first to examine the fracture process in a systematic way. They applied uniaxial strain at different pull-rates to a glass sample of few thousand atoms and did a detailed analysis of the effect of the strain-rates on the stress–strain curves. The application of uniaxial strain was uniform throughout the sample, unlike the way Soules and Busby applied strain to their samples. Initially, Ochoa and Simmons used the S-potential and observed that the fracture strength of the glass increased with increasing strain. They attributed this to the fact that at lower strain-rates the system has more time to relieve its strain by structural rearrangement of atoms. In their stress–strain plots, one could identify four distinct regions; (i) the elastic regime where stress increased linearly with strain, (ii) a yield region where the stress varied very slowly with strain, (iii) a region where there was a dramatic drop in the stress with increasing strain and finally (iv) separation of the material corresponding to zero stress. Later, Swiler and co-workers [7,8] extended these results by looking at void formation and coalescence and concluded that 'at low strain rates, strain added uniformly to the structure is allowed to flow from higher-density regions to lower density regions. This effect leads to coalescence of voids eventually causing fracture propagation through the simulated structure'. In addition they also estimated the size of a critical void to be 4.5 Å and linked the fracture process to the 'availability of free volume'. An examination of the fractured surface revealed that it was oxygen-rich. In another paper [9], these same authors examined the effect of thermal vibrations and found these vibrations induced individual tetrahedra to rotate and orient along the strain direction. In addition, the simulations were repeated using the FG potential; there was no difference in the observed behavior of the 'strained' glass samples, leading to an important conclusion that the fracture-controlling processes were 'potential independent'.

Van Brutzel et al. [12] performed multi-million atom simulations on a-SiO_2 to study the propagation of a crack in the medium. They used the V-potential and were able to see the growth and coalescence of voids and pores (~50–60 Å in radius) near the crack tip due to localization of strain around the crack tip. In their studies, a V-shaped notch was created on one edge of the simulation box and the box was then subjected to an external strain by displacing atoms in the top and bottom layers of the box. The effect of temperature on crack propagation was studied and it was found that some voids grew further away from the crack tip at higher temperatures, leading to secondary crack growth. They concluded that at lower temperatures (~300 K) the strain energy was dissipated along the crack tip, and at higher temperatures (>1000 K) the strain energy was also dissipated in the formation and growth of pores into a secondary crack. Further, crack branching was observed and an average crack velocity was also reported. The same set of simulations was repeated for nanostructured silica glass and pore formation was observed in the intergranular regions. Crack fronts then coalesce with these pores causing intergranular failure.

Zhu et al. [49] using a novel method that integrated elements of ab initio calculations with classical MD simulations, studied the fracture characteristics of SiO_2 'nanorods'. Their work consisted of using quantum-level MNDO calculations (explained in Ref. [51]) to obtain forces on atoms, and MD to solve for the equations of motions of atoms at every MD time step. As they used a silica nanostructure which was not indicative of amorphous structure, the resultant fracture strength was much greater than that seen in a-SiO_2.

In almost all of the work that has been reviewed, a common theme has been the formation and coalescence of voids and pores that eventually leads to failure of the strained glass sample. Recent experimental evidence seems to show that brittle fracture at the nanoscale is indeed via formation and coalescence of voids [15]. Thus the above agreement between the simulation and experimental results is very significant and in particular, is of generic importance from a simulation point of view, given the fact that the research teams used different simulation procedures. The methods of Simmons et al. and Van Brutzen and co-workers were in fact markedly different, the former studying the effects of strain on a small sample of few thousand atoms while the latter using more than a million atoms to obtain their results. Another important difference was the fact that while Simmons et al. were over-constraining their samples by applying uniform strain throughout a homogenous sample, Van Brutzen et al. only displaced the boundary atoms of a 'pre-cracked' sample. Thus the former were fracturing their samples about 20% strain, while the latter were able to rupture the glass at about 6.5% strain, for a strain rate of 0.01/ps. Additionally, the potential being employed were also different. In summary, Table 1 lists the fracture strength and the Young's modulus of silica glass when simulated using the various potentials as well as the experimental values.

In spite of the fact that a very important issue – that of void coalescence leading to failure has been

Table 1
Comparison of fracture strengths and Young's modulus of simulated silica glasses with experimental values

System	Maximum strength/strain rate (GPa)/ps	Young's modulus (GPa)
S-potential	24–35 (0.05–0.5)	~220
BMH	30–65 (0.2–8.0)	~220
FG	12–21 (0.05–0.5)	~125
BKS	15–22 (0.005–0.1)	~100
Experiment	18	71.9

established, a few other key issues were either neglected or ignored. Though Swiler et al. could identify a 'critical void', a methodical look at the growth of the void was not undertaken. The open network structure of a-SiO_2 gives rise to voids of different sizes. Thus a systematic study of the evolution of the void-size distributions as a function of strain-rate (and therefore strain) would be extremely beneficial as one could then correlate it to the stress–strain curves and characterize the different regions in the stress–strain plots. Charge-transfer between atoms is also an important aspect that has to be examined. In addition, based on the above discussed results, though one could infer that voids form due to local stress/strain concentrations, the mechanism behind void growth has not yet been identified. This is of enormous significance as then we can clearly characterize the extensive atomic rearrangement that takes place around the propagating crack tip.

6. Recent progress

The discussion in the previous sections clearly identified the need to 'fill in the blanks' in the current models describing atomic-level fracture processes in brittle materials. The following section will address some of these issues; specifically, we look at the evolution of critical voids as a function of strain for all strain-rates. The effect of charge-transfer will be documented and the importance of charge-transfer will be discussed. Structural rearrangement in 'critical regions' will also be briefly scrutinized.

6.1. Simulation procedure

In our studies, we use a modified BKS potential [38] to model the interactions between atoms. The modification is necessary to prevent an unphysical divergence at very small distances of separation between atoms. The modified BKS potential has the form

$$\phi_{ij} = \frac{q_i q_j}{r_{ij}} + A_{ij}\exp(-b_{ij}r_{ij}) - \frac{c_{ij}}{r_{ij}^6} + 4\varepsilon_{ij}\left[\frac{\sigma_{ij}}{r_{ij}}\right]^{24} - 4\varepsilon_{ij}\left[\frac{\sigma_{ij}}{r_{ij}}\right]^{6},$$

where ϕ_{ij} is the potential energy corresponding to an interatomic separation of r_{ij}. A_{ij}, b_{ij}, c_{ij}, ε_{ij} and σ_{ij} are given in Table 2.

Table 3
Charge-transfer parameters

q_{si} (q_i)	q_0 (q_j)	Δq	R_{ab}	ξ
4.0	−2.0	0.4523	1.90	0.29

For our charge-transfer studies, we use the formulation of Alavi et al., in conjunction with the modified BKS potential to obtain the 'CTBKS' potential. Net charges on each atom are obtained by the following equation:

$$q_i = q_i^a - \Delta q \sum_j \frac{1}{2}\left[1 - \tanh\left(\frac{R_{ij} - R_{ab}}{\xi}\right)\right],$$

$$q_j = q_j^b + \Delta q \sum_i \frac{1}{2}\left[1 - \tanh\left(\frac{R_{ij} - R_{ab}}{\xi}\right)\right].$$

The charge-transfer parameters (listed in Table 3) in the above equation are chosen so that in the fully coordinated equilibrated state, all Si and O atoms have a net charge equaling that prescribed by the BKS potential (+2.4, and −1.2 respectively), and in the zero-coordinated state, an Si atom has a charge of +4, and an O atom has a charge of −2.

The simulation studies were carried out on samples that were prepared using the 'recipe' prescribed by Huff et al. [50]. Initially, a low-cristobalite BKS sample of 3528 atoms (1176 Si and 2352 O) was melted at 8000 K and was step-wise quenched all the way down to 300 K. It was then equilibrated to ensure zero pressure. The resultant glass obtained had a mass density of 2.2 g/cc, very close to that of experiment. The same procedure was carried out by including charge-transfer and the equilibrated glass sample had a slightly higher density of 2.3 g/cc. Both samples were cubic, the dimensions for the BKS glass being $37 \times 37 \times 37$ Å^3, while the dimensions for the CTBKS glass equaled 36.34 Å in each direction. Following the method of Simmons et al., the samples were uniformly strained at different uniaxial strain rates ranging from 0.1/ps to 0.005/ps. All simulations were carried out at 300 K, the temperature maintained via a Nose–Hoover thermostat [51]. The size of the MD time step used was one femtosecond and the equations of motion of the atoms were solved using a Verlet–Beeman integrator [52]. The MD box was subjected to periodic boundary conditions in all simulation runs. Ewalds summation [53] was used, to ensure a rapid

Table 2
Parameters used in the modified BKS potential

Interaction type	Parameter				
	A_{ij} (eV)	b_{ij} (Å^{-1})	c_{ij} (eV/Å^6)	ε_{ij} (eV)	σ_{ij} (Å)
Si–O	18003.7572	4.8732	133.5381	1.12245×10^{-2}	1.3100
O–O	1388.7730	2.7600	175.0000	3.5653×10^{-4}	2.2000
Si–Si	–	–	–	12.6387	0.4200

convergence of the coulombic contribution to the total potential energy of the system. Virial stresses were calculated in order to obtain the stress–strain relations for all strain rates. Radial distribution functions (RDF), bond-angle distributions (BAD) were periodically recorded during the simulation runs. In addition, we used the method of void analysis to characterize the local differences in densities of the various samples at the atomic-scale. A discussion of the analysis is given below.

6.2. Void analysis

Generally speaking, a void can be defined to be a region enclosing empty space. For simplicity, in this work, it is assumed that the voids are spherical in shape. Also, we assume that the atoms are point particles and therefore do not associate any volume with the atoms. The algorithm to compute the void size distribution is as follows: The MD box is divided into a very fine grid such that the distance between neighboring grid points is much smaller than the typical Si–O first neighbor distance (~1.6 Å). At every grid point, the distance to the nearest atom is calculated; this signifies the void radius at that given grid point. If this is smaller than a cutoff (~1.6 Å) then this grid point is automatically neglected, otherwise the coordinates of this grid point is retained. Once the entire grid-space is scanned, the algorithm then checks for overlap of grid points. In other words, if a grid point lies within the void radius of another grid point, then the former grid point is immediately rejected. This approach automatically allows one to locate the center of the biggest void enclosed in that region and therefore a region devoid of atoms and of arbitrary shape is represented by a series of non-overlapping spherical voids.

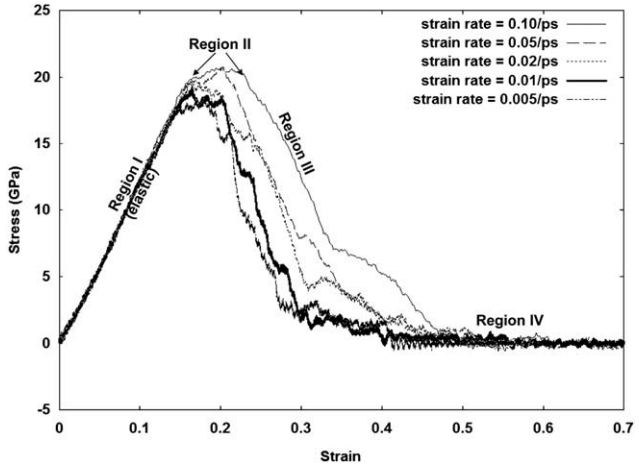

Fig. 1. Uniaxial stress–strain curves for the BKS glass. The 'region' labels are specific for the 0.10/ps case.

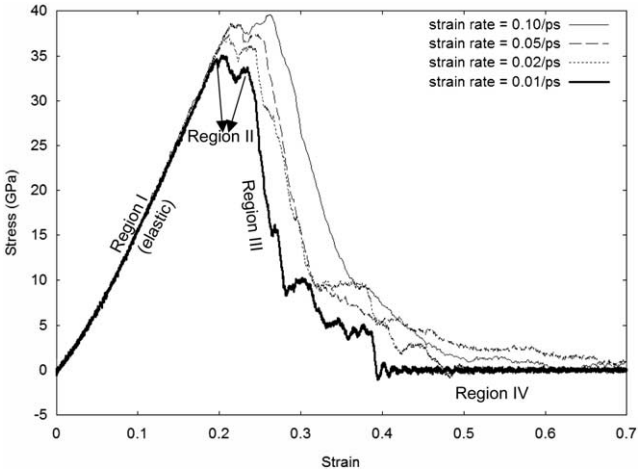

Fig. 2. Uniaxial stress–strain curves for the CTBKS glass. The 'region' labels are specific for the 0.01/ps case.

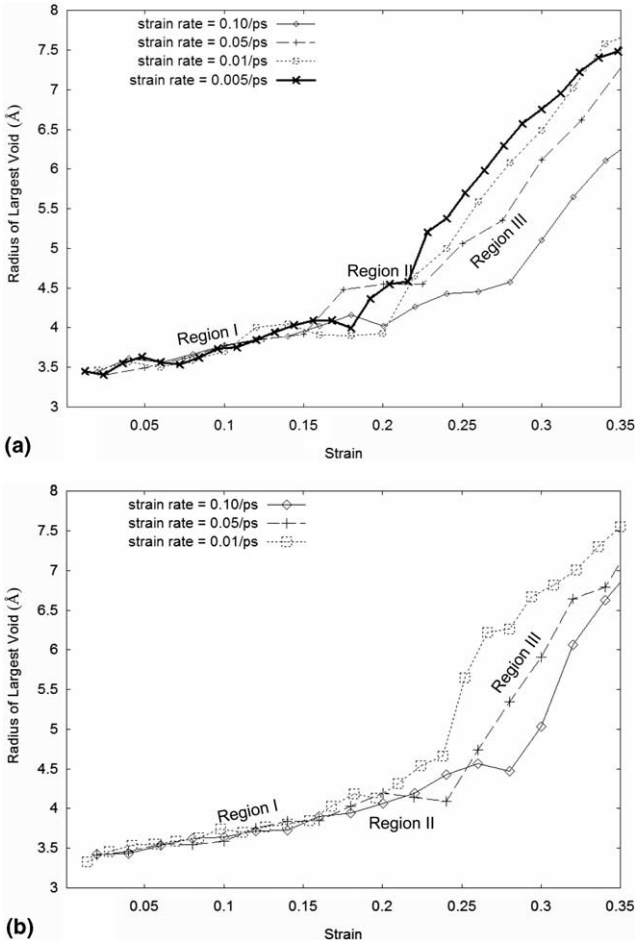

Fig. 3. (a) Growth of the critical void (BKS) as a function of strain for different strain-rates at 300 K. (b) Growth of the critical void (CTBKS) as a function of strain for different strain-rates at 300 K. The 'region' labels are specific for the 0.05/ps case.

7. Results and discussions

The uniaxial stress–strain curves for both BKS as well as CTBKS glasses are represented in Figs. 1 and 2 respectively. By examining both figures, it is clear that in each case, the stress–strain curves behave exactly as that observed by Simmons et al.; (i) each stress–strain curve has four distinct regions (as shown in the figures), and (ii) the fracture strength increases with increasing strain-rate.

A comparison of both figures shows that CTBKS glasses are much stronger than the 'normal' BKS glasses. This is a direct consequence of the way we had set up charge-transfer to proceed as we strained the sample. In other words, the system is inherently biased to resist the straining of Si–O bonds, as the magnitude of charge increases on both atoms with increasing Si–O bond lengths, thereby making the coulombic term much stronger. It would have been instructive as well as informative to study the charge-transfer behavior of glasses under strain, where the net charge on an atom goes to zero when all atomic bonds are broken for the given atom. We have investigated such glasses, but the resulting glasses were very weak and their densities were much smaller than the experimental densities. However, the more important outcome is the fact that the stress–strain behavior for both CTBKS and BKS glasses are similar and only differ in a scaling factor (proportional to the Si–O bond strength). Thus it would be very reasonable to expect that the fracture mechanisms as such will not be drastically affected by charge-transfer effects. In the

Table 4
Extent of each 'stress–strain' region for the BKS glass as a function of strain-rate

Strain-rate	Range of strain			
	Region I	Region II	Region III	Region IV
0.1/ps	0–0.16	0.16–0.23	0.23–0.50	>0.50
0.05/ps	0–0.16	0.16–0.22	0.22–0.48	>0.48
0.01/ps	0–0.16	0.16–0.20	0.20–0.30	>0.30
0.005/ps	0–0.15	0.15–0.18	0.18–0.27	>0.27

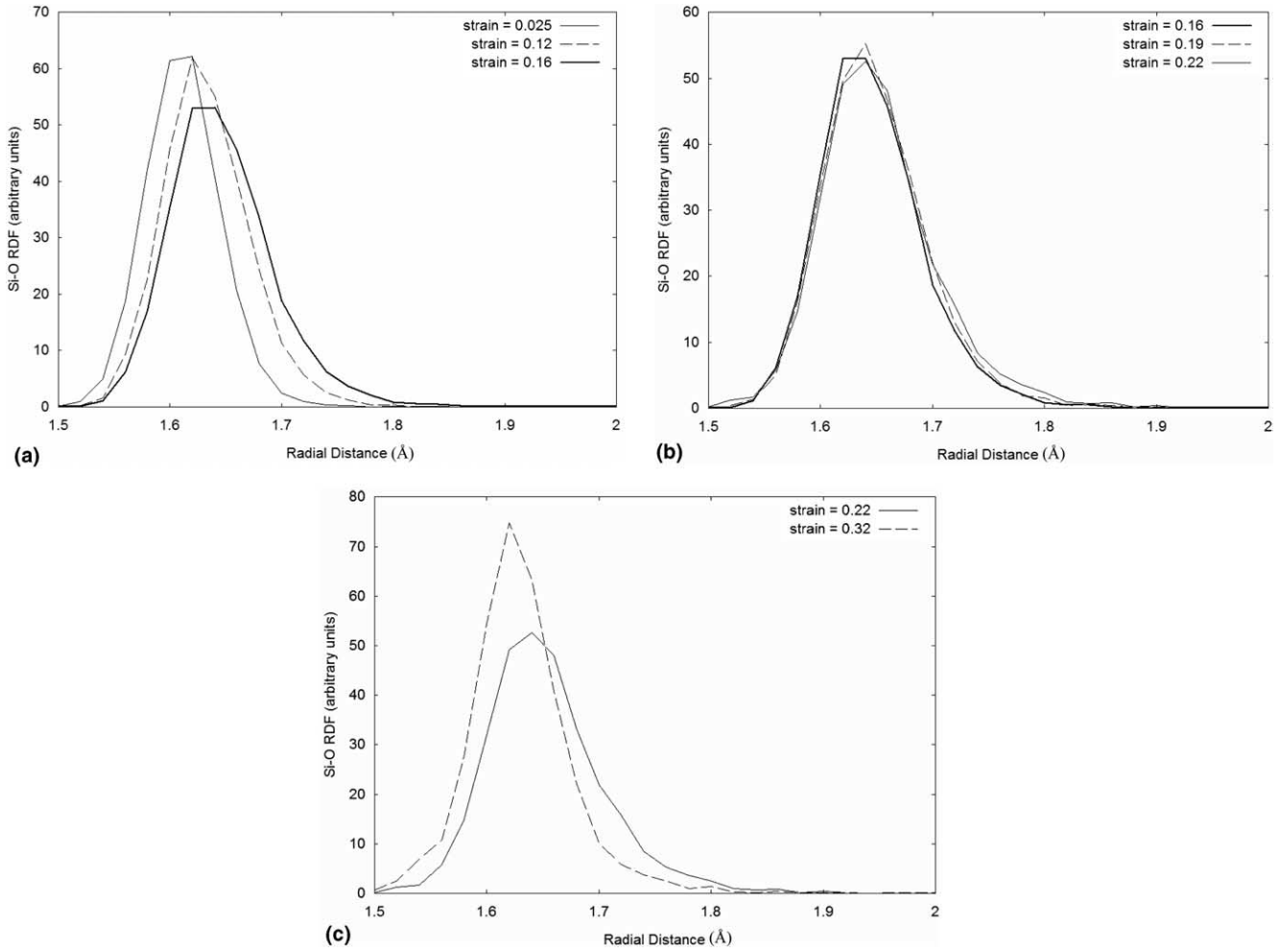

Fig. 4. Evolution of the 'BKS' first neighbor Si–O RDF's in region I (a), region II (b) and region III (c) as a function of strain at a strain-rate = 0.05/ps.

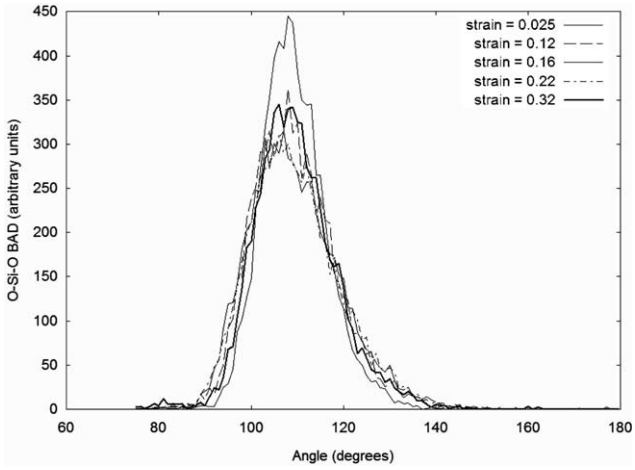

Fig. 5. Evolution of the 'BKS' O–Si–O bond-angle distribution (BAD) as a function of strain at a strain-rate = 0.05/ps.

following paragraphs, we report on the evolution and growth of voids and try to correlate them to previous results.

Fig. 3(a) and (b) shows the radius of the biggest void (BV) as a function of strain for all strain-rates for the BKS and CTBKS glasses respectively. Let us first examine the case when charge-transfer is 'turned off'. As previously stated, each stress–strain curve has four distinct regions, the final (fourth) region corresponding to an already separated sample (zero-stress region). The more important regions are the first three distinct parts of the curve. Consider Fig. 3(a) which depicts the evolution of BV at all strain-rates. For every strain-rate one can define three distinct regions (I, II and III), very similar to the corresponding stress–strain curves. Region I is characterized by a gradual growth in the size of BV. In region II, the growth is muted and the increase in size of BV with increasing strain is not as noticeable as it is in region I. This is followed by a rapid increase in the size of BV (region III). The limits of each region (i.e. the strain interval over which each region is defined) in both Figs. 1 and 3(a) are almost identical and can be easily related to each other. The limits of each region in both Figs. 1 and 3(a) are tabulated in Table 4.

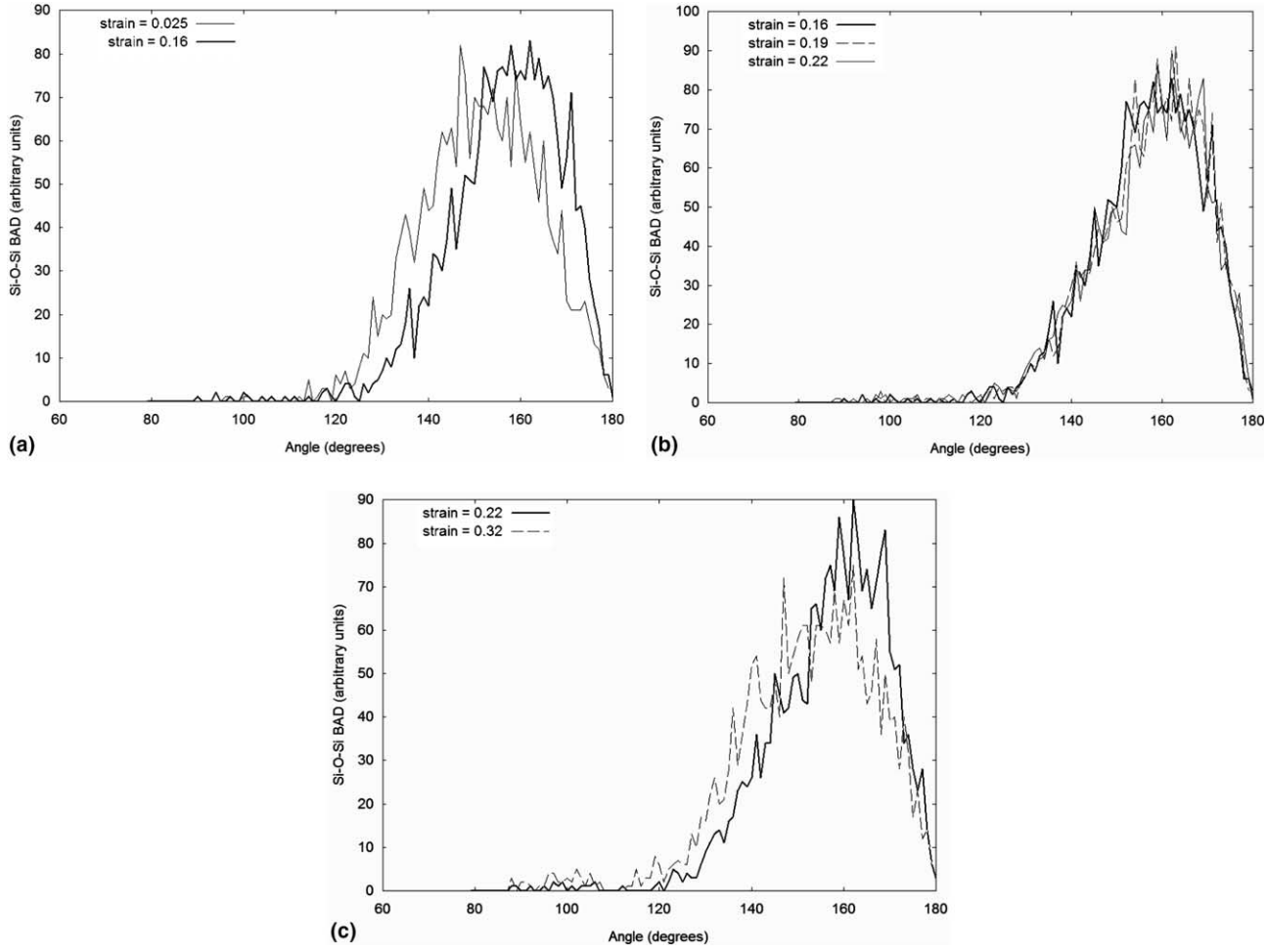

Fig. 6. (a) Evolution of the 'BKS' Si–O–Si bond-angle distribution (BAD) in region I (a), region II (b) and region III (c) as a function of strain at a strain-rate = 0.05/ps.

Thus region I in Fig. 3(a) can be related to the elastic deformation of voids, the voids growing via the extension of Si–O bonds. In region II, the fact that the size of BV does not vary much, combined with the fact that the stress is almost strain independent, implies that the excess strain might be distributed in such a way that only smaller voids grow, via structural rearrangement rather than the elastic stretching of Si–O bonds. If the above was not true, then we would have seen a further linear increase of stress with strain. Once a critical distribution of voids is achieved, coalescence occurs and BV grows very rapidly (region III). This ultimately leads to separation of the material.

Having identified three distinct regions in Figs. 1 and 3(a), we can define the size of a 'critical void' to be the size of BV at the 'onset' of region III. Onset occurs at strains that increase with increasing strain-rate (around 0.18 for 0.005/ps, all the way to 0.23 for 0.1/ps). The size of the critical voids is also a function of strain-rate, the critical radius being about 4 Å for lower strain-rates (0.005 and 0.01/ps) and around 4.5 Å for the higher strain-rates (0.05 and 0.1/ps). Similar conclusions can be drawn for the CTBKS glass too, though there are some minor differences (see Fig. 3(b)). Region II extends over a smaller range of strain, while the onset strain occurs at a larger strain with respect to the BKS glass for a given strain-rate.

In order to further confirm some of our observations, we looked at the RDF's, and the BAD's as a function of strain for a representative strain-rate (0.05/ps) for the BKS glass. Fig. 4(a)–(c) represents the first-neighbor Si–O RDF at different strains. In Fig. 4(a), the Si–O peak shifts to larger distances of separation with increasing strain, corresponding to region I behavior, where there is elastic stretching of the Si–O bonds. Between strains of 0.16 and 0.22, the RDF distributions are very similar (as shown in Fig. 4(b)), implying that the strain is definitely not used up in extending the Si–O bonds further. This clearly lends more support to the idea that in region II, the external strain applied aids in some sort of atomic rearrangement without a change in Si–O bond length. Fig. 4(c) represents the fact that in region III there is 'bulk recovery', as at a much higher strain (0.325), the Si–O peak shifts back to 1.6 Å, corresponding to an unstrained Si–O bond length. Figs. 5 and 6 illustrate the variation in BAD's (both O–Si–O and Si–O–Si) with strain. A comparison between both figures indicates that while the O–Si–O BAD does not vary much with increasing strain, there is a discernable difference in Si–O–Si BAD as a function of strain. Specifically, within the elastic region, the Si–O–Si peak shifts from about 144° all the way up to 163° (Fig. 6(a)), where it remains static over an interval of strain (corresponding to region II – Fig. 6(b)), and then moves back to a less-strained bond angle (region III – Fig. 6(c)).

The above observations could clearly identify and characterize the stress–strain curves by correlating them to the growth of voids as well as the evolution of RDF's and BAD's. In addition, a careful interpretation of the results enabled us to shed new light on the evolution of voids. The interpretation was an important exercise to characterize the fracture process; nevertheless further analysis was required in order to describe atomic rearrangement in critical regions enveloping large voids – 'regions of low atomic densities'. In order to locate these low-density regions, we divided the MD box into cells perpendicular to the direction of uniaxial strain and periodically recorded the number of atoms in each cell as a function of strain. Once the region where separation of the material occurs was identified (corresponding to low atomic density), a systematic look at average local coordination and average local BAD's and RDF's as a function of strain was undertaken. Of most interest was the variation of the average local Si–O–Si BAD with strain in the critical cells. An important point has to be

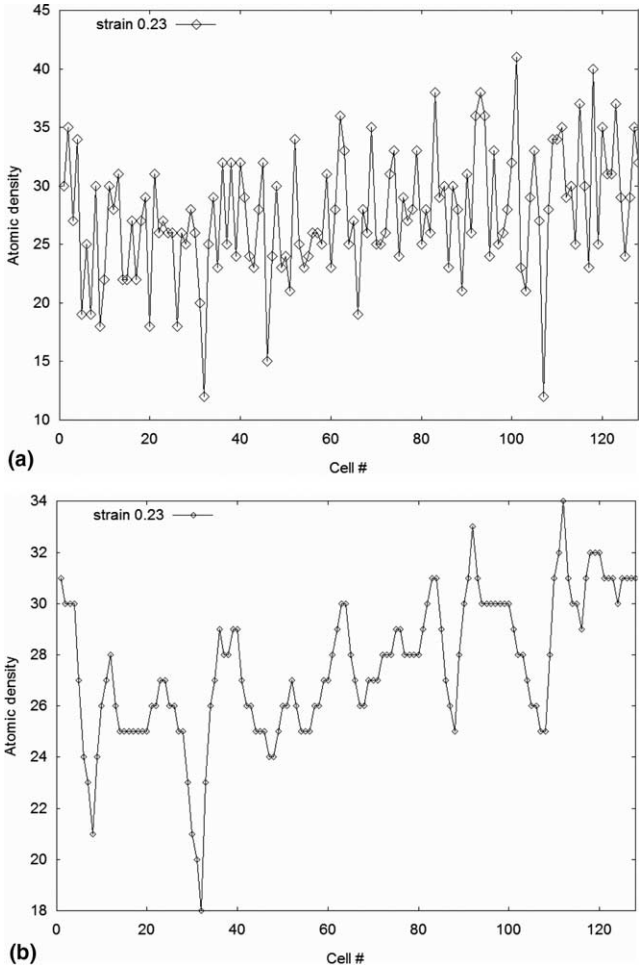

Fig. 7. (a) 'Raw' atomic density distribution obtained at strain = 0.23 for a strain-rate = 0.05/ps for 'BKS' glass. (b) Wavelet transformed atomic density distribution at strain = 0.23 for a strain-rate = 0.05/ps for 'BKS' glass.

noted; since the atomic density distribution was very noisy, we 'cleaned' up the 'signal' using wavelet transforms, which eliminates noise by averaging it out. Wavelet transforms are extremely powerful tools finding great uses in signal processing. A detailed description of the technique is beyond the scope of this paper, and readers can find more information in Ref. [54].

Using the same 'representative' case for our analysis (strain-rate = 0.05/ps for BKS), the change in local atomic densities as a function of strain was examined. The Daubechies wavelet functions were used as the basis functions for the wavelet transforms, and the number of cells equaled 128. Just beyond the onset of region III (strain = 0.23), we obtained both the 'raw' atomic density distribution (Fig. 7(a)) as well as its wavelet-transformed signal (Fig. 7(b)). Fig. 7(b) clearly shows the region of interest lies between cell 20 and cell 40, which is not readily obvious from Fig. 7(a). Having located the critical region, the average Si–O–Si BAD was examined as a function of strain. The average Si–O–Si bond angle is calculated by first picking out the O atoms and its Si neighbors in each cell and then averaging the Si–O–Si bond-angle value over all O atoms.

Fig. 8(a) and (b) depict the evolution of the wavelet transformed local Si–O–Si BAD with strain. From Fig. 8(a), one can deduce that at strain 0.23 (just beyond the onset strain), the Si–O–Si BAD in the region of interest (cells 20–40) is highest with respect to other regions. At a much higher strain (=0.40), it drops down to a value between 90° and 100° (Fig. 8(b)), once again markedly different from the rest of the material, only much smaller. The above observations indicate that one can characterize the 'critical' regions by looking at the local BAD. In the initial stages of fracture, the Si–O–Si BAD in the 'critical' regions are much more strained (as evident by the large bond angles), while in the later stages of fracture, the atoms in the critical regions rearrange such that the corresponding Si–O–Si BAD drops to about 90°.

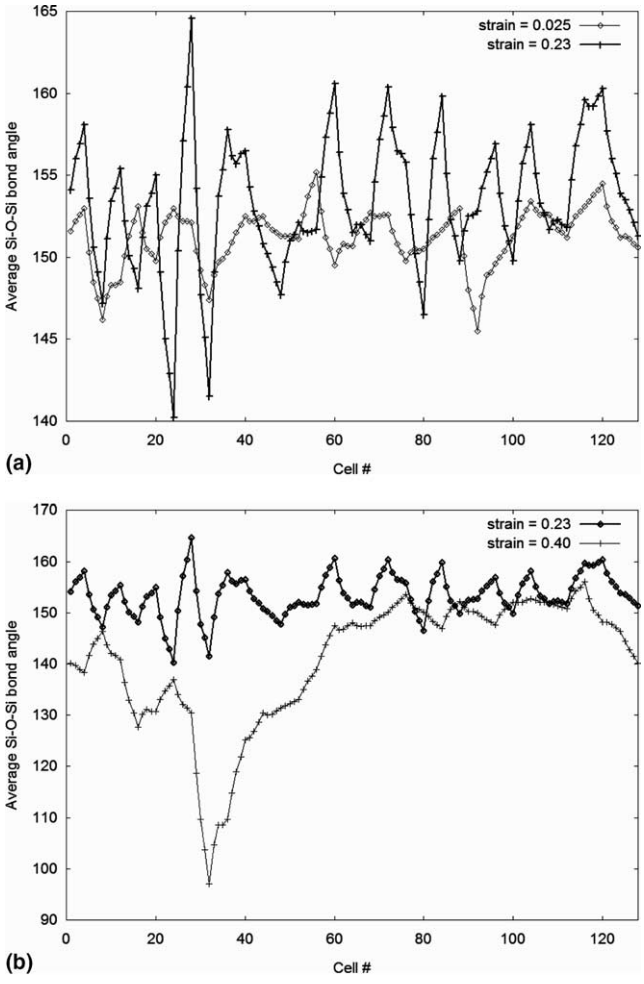

Fig. 8. (a) Comparison of wavelet transformed distribution of the average local Si–O–Si bond angles at the initial stage (strain = 0.025) and at an intermediate stage of fracture (strain = 0.23) for a strain-rate = 0.05/ps for 'BKS' glass. (b) Comparison of wavelet transformed distribution of the average local Si–O–Si bond angles at strain = 0.23 and at a later stage of fracture (strain = 0.40) for a strain-rate = 0.05/ps for 'BKS' glass.

8. Conclusions

The main focus of this paper was to review past MD investigations of the brittle fracture process in a-SiO_2 and to address some of the key issues ignored by the above works. We analyzed the effect of charge-transfer on our fracture studies by using an empirical model (CTBKS) in conjunction with the 'BKS' potential. The CTBKS glasses were much stronger than the regular 'BKS' glasses, but the fundamental mechanisms governing fracture in both cases were identical. A systematic look at the evolution of 'critical' voids was undertaken and this was used to characterize the stress–strain curves obtained when the glass sample was subjected to uniaxial strain at varying rates. In addition, 'soft' regions in the glass sample were identified by looking at local bond-angle distributions. These regions were characterized by high Si–O–Si bond angles prior to failure.

Acknowledgements

This work was supported in part by the U.S. National Science Foundation under ITR award DMR-0325553.

References

[1] A.A. Griffith, Philos. Trans. R. Soc. A 221 (1921) 163.
[2] G.R. Irwin, J. Appl. Mech. 24 (1957) 361.
[3] G.I. Barenblatt, Adv. Appl. Mech. 7 (1962) 55.
[4] T.F. Soules, R.F. Busbey, J. Chem. Phys. 78 (10) (1983) 6307.

[5] G.J. Dienes, A. Paskin, J. Phys. Chem. Solids 48 (11) (1987) 1015.
[6] R. Ochoa, J.H. Simmons, J. Non-Cryst. Solids 75 (1985) 413.
[7] R. Ochoa, T.P. Swiler, J.H. Simmons, J. Non-Cryst. Solids 128 (1991) 57.
[8] J.H. Simmons, T.P. Swiler, R. Ochoa, J. Non-Cryst. Solids 134 (1991) 179.
[9] T.P. Swiler, J.H. Simmons, A.C. Wright, J. Non-Cryst. Solids 182 (1995) 68.
[10] T.P. Swiler, T. Varghese, J.H. Simmons, J. Non-Cryst. Solids 181 (1995) 238.
[11] F.F. Abraham, D. Brodbeck, R.A. Rafey, W.E. Rudge, Phys. Rev. Lett. 73 (2) (1994) 272, and references therein.
[12] L. Van Brutzel, C.L. Rountree, R.K. Kalia, A. Nakano, P. Vashishta, Mater. Res. Soc. Symp. Proc. 703 (2002) 117.
[13] C.L. Rountree, R.K. Kalia, E. Lidorikis, A. Nakano, L. Van Brutzel, P. Vashishta, Annu. Rev. Mater. Res. 32 (2002) 377, and references therein.
[14] R. Ochoa, M. Arief, J.H. Simmons, Mater. Res. Soc. Symp. Proc. 703 (2002) 105.
[15] E. Guilloteau, H. Charrue, F. Creuzet, Europhys. Lett. 34 (7) (1996) 549.
[16] F. Celarie, S. Prades, D. Bonamy, L. Ferrero, E. Bouchaud, C. Guillot, C. Marliere, Phys. Rev. Lett. 90 (7) (2003) 075504.
[17] S.M. Wiederhorn, J. Am. Ceram. Soc. 50 (1967) 407.
[18] S.M. Wiederhorn, L.H. Bolz, J. Am. Ceram. Soc. 53 (1970) 543.
[19] B.A. Proctor, Phys. Chem. Glass. 31 (2) (1990) 78.
[20] J.E. Gordon, D.M. Marsh, M.E.M.L. Paratt, Proc. R. London Ser. A 249 (1959) 59.
[21] J.M. Haile, Molecular Dynamics Simulation, Wiley/Interscience, 1992.
[22] M. Wilson, T.R. Walsh, J. Chem. Phys. 113 (20) (2000) 9180.
[23] T.R. Walsh, M. Wilson, A.P. Sutton, J. Chem. Phys. 113 (20) (2000) 9191.
[24] W. Wong-Ng, G.S. White, S.W. Freiman, J. Am. Ceram. Soc. 75 (11) (1992) 3097.
[25] J.K. West, L.L. Hench, J. Mater. Sci. 29 (1994) 3601.
[26] R.L. Erikson, C.J. Hostelter, Geochim. Cosmochim. Acta 51 (1987) 1209.
[27] M. Schaible, Crit. Rev. Solid State Mater. Sci. 24 (4) (1999) 265.
[28] L.V. Woodcock, C.A. Angell, P. Cheeseman, J. Chem. Phys. 65 (1976) 1565.
[29] T.F. Soules, J. Chem. Phys. 71 (1979) 4570.
[30] S.K. Mitra, M. Amini, D. Fincham, R.W. Hockney, Philos. Mag. 43 (1981) 365.
[31] S.K. Mitra, Philos. Mag. 45 (1982) 529.
[32] S.K. Mitra, J.M. Parker, Phys. Chem. Glass. 25 (1984) 95.
[33] B.P. Feuston, S.H. Garofalini, J. Chem. Phys. 89 (1988) 5818.
[34] P. Vasishta, R.K. Kalia, J.P. Rino, I. Ebbsjo, Phys. Rev. B 41 (17) (1990) 12197.
[35] B. Vessal, M. Amini, C.R.A. Catlow, J. Non-Cryst. Solids 159 (1993) 184.
[36] A.C. Wright, J. Non-Cryst. Solids 159 (1993) 264.
[37] S. Tsuneyuki, M. Tsukada, H. Aoki, Y. Matsui, Phys. Rev. Lett. 61 (7) (1988) 869.
[38] B.W.H. van Beest, G.J. Kramer, R.A. van Santeen, Phys. Rev. Lett. 64 (16) (1990) 1955, the modification to the BKS potential was suggested by L.R. Corrales, private communication.
[39] S. Tsuneyuki, M. Tsukada, H. Aoki, Y. Matsui, Phys. Rev. Lett. 64 (1990) 776.
[40] J.R. Rustad, D.A. Yuen, F.J. Spera, Phys. Rev. A 42 (1990) 2081.
[41] J.S. Tse, D.D. Klug, J. Chem. Phys. Phys. 95 (1991) 9176.
[42] R.G. Della Valle, H.C. Andersen, J. Phys. Chem. 94 (1991) 5056.
[43] R.G. Della Valle, H.C. Andersen, J. Phys. Chem. 97 (1992) 2682.
[44] L. Huang, J. Keiffer, J. Phys. Chem. 118 (2003) 1487.
[45] A. Alavi, L.J. Alvarez, S.R. Elliot, I.R. McDonald, Philos. Mag. B 65 (3) (1992) 489.
[46] F.H. Streitz, J.W. Mintmire, Phys. Rev. B 50 (16) (1994) 11996.
[47] S.M. Valone, S.R. Atlas, J. Chem. Phys. 120 (2004) 7262.
[48] J. Kieffer, C.A. Angell, J. Non-Cryst. Solids 106 (1988) 336.
[49] T. Zhu, J. Li, S. Yip, R.J. Bartlett, S.B. Trickey, N.H. de Leeuw, Molec. Simul. 29 (2003) 671.
[50] N.T. Huff, E. Demiralp, T. Cagin, W.A. Goddard III, J. Non-Cryst. Solids 253 (1999) 133.
[51] S. Nose, Prog. Theor. Phys. Suppl. 103 (1991) 1.
[52] D. Beeman, J. Comput. Phys. 20 (2) (1976) 130.
[53] P. Ewald, Ann. Phys. 64 (1921) 253.
[54] I. Daubechies, Ten Lectures on Wavelets, SIAM, Philadelphia, PA, 1992.